



De-Tumbling & Earth Pointing of a 6U Spacecraft

Spacecraft Attitude Dynamics & Control (A.Y. 2019/20)

Massimo Piazza (919920)

massimo.piazza@mail.polimi.it

Contents

1	Introduction	1
2	ADCS Architecture	2
2.1	Attitude Sensors	2
2.1.1	Gyroscope - STIM202 (<i>Sensoror, AS</i>)	2
2.1.2	Sun Sensor - SS200 (<i>Hyperion Technologies, B.V.</i>)	2
2.1.3	Earth Horizon Sensor - MAI-SES (<i>Maryland Aerospace, Inc.</i>)	2
2.2	Actuators	2
2.2.1	Magnetorquers - NCTR-M012 (<i>NewSpace Systems, Ltd.</i>)	2
2.2.2	Control Moment Gyros (<i>Honeybee Robotics, Ltd.</i>)	2
3	Model Description	3
3.1	Spacecraft Dynamics	3
3.1.1	Attitude Dynamics	3
3.1.2	Orbital Mechanics	3
3.2	Disturbance Torques	3
3.2.1	Atmospheric Drag	3
3.2.2	Solar Radiation Pressure	4
3.2.3	Earth's Magnetic Field	4
3.2.4	Gravity Gradient	4
3.3	Attitude Sensors	5
3.3.1	Gyroscope	5
3.3.2	Sun Sensor & Earth-Horizon Sensor	5
3.4	Actuators	5
3.4.1	CMGs	5
3.4.2	Magnetorquers	6
4	Control & Determination Algorithms	7
4.1	Control Laws	7
4.1.1	De-Tumbling	7
4.1.2	Tracking: Earth Pointing	7
4.2	Attitude Determination Algorithm	7
4.3	Noise Filtering	8
5	Results	9
5.1	Disturbance Torques	9
5.2	De-Tumbling	10
5.2.1	Dynamics	10
5.2.2	Control	11
5.3	Earth Pointing	12
5.3.1	Dynamics	12
5.3.2	Control	14
6	Conclusions	15

Nomenclature

Nondimensional Quantities

\mathcal{J}	Wabha's cost function	[—]
C_D	Drag coefficient	[—]
e	Eccentricity	[—]

Physical Quantities

β	Gimbal motor inclination	[deg]
δ	CMG tilt angle	[deg]
μ	Gravitational parameter	[km ³ /s ²]
Ω	RAAN	[deg]
ω	Argument of periapsis	[deg]
ρ	Density	[kg/m ³]
θ	True anomaly	[deg]
$\underline{\omega}$	Angular velocity	[rad/s]
\underline{b}	Earth's magnetic field	[T]
\underline{d}	Disturbance torque	[N · m]
\underline{m}	Magnetic dipole	[A · m ²]
\underline{r}	Position vector	[m]
\underline{u}	Control torque	[N · m]
\underline{v}	Velocity vector	[m/s]
A	Surface area	[m ²]
a	Semi-major axis	[km]
$A_{B/N}$	Attitude matrix	[—]
c	Speed of light	[m/s]
F_e	EM power per unit surface	[W/m ²]
G	Gravitational constant	[m ³ /(kg · s ²)]
h	Angular momentum	[N · m · s]
i	Inclination	[deg]
J	Inertia matrix	[kg · m ²]
m_{earth}	Earth's mass	[kg]

p Semi-latus rectum [km]

t Time [s]

Subscripts/Superscripts

B Body frame

d Desired

e Error

L LVLH frame

N Inertial frame

R Rotor

Acronyms

ADCS	Attitude Determination & Control Subsystem
ARW	Angular Random Walk
CG	Center of Gravity
CMG	Control Moment Gyro
CP	Center of Pressure
DCM	Direction Cosine Matrix
ECI	Earth-Centered Inertial
EH	Earth-Horizon
FoV	Field of View
GG	Gravity Gradient
LPF	Low Pass Filter
MT	Magnetic Torquer
PF	PeriFocal
RRW	Rate Random Walk
S/C	SpaceCraft
SRP	Solar Radiation Pressure
SS	Sun Sensor
w.r.t.	with respect to

1 Introduction

In this report, the attitude dynamics and control of a **6U** spacecraft in LEO environment will be investigated. The simulation will account for the presence of disturbance torques along with the actual performance of the selected ADCS components.

A preliminary estimation of **mass properties** has been carried out, based on the model in Fig. 1.

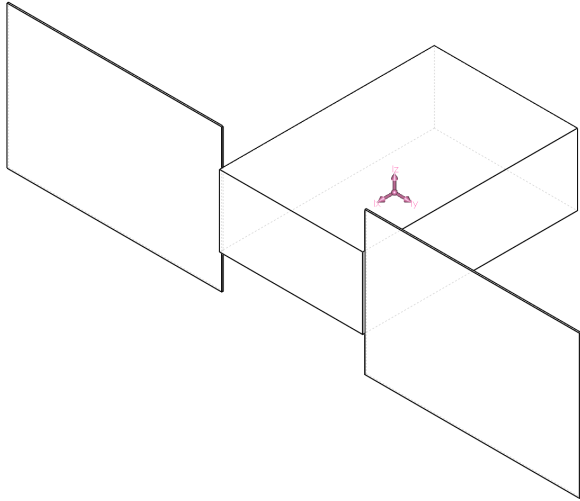


Figure 1: Model of the 6U cubesat

Environmental disturbances are computed in correspondence of the reference **orbit** reported in Tab. 2.

Table 1: Mass and size of the S/C

	Mass [kg]	Size [m]
Main body	9.0	$0.3 \times 0.2 \times 0.1$
Solar panels (single panel)	0.6	0.3×0.2

$$J = \begin{bmatrix} 0.09 & 0 & 0 \\ 0 & 0.14 & 0 \\ 0 & 0 & 0.07 \end{bmatrix} \text{ kg} \cdot \text{m}^2$$

$$x_{\text{CG}} = [0.01 \ 0 \ 0]^T \text{ m}$$

Table 2: Initial orbital elements

a	e	i	Ω	ω	θ_0
6971 km	0.1	10°	80°	123°	0°

The S/C is equipped with

- **attitude sensors:** Sun sensor + Earth-horizon sensor + gyroscope
- **actuators:** a set of 3 magnetic torque rods + a set of 4 control moment gyros

Our analysis will dwell on three main aspects:

- modeling and characterization of environmental **disturbances**
- **de-tumbling** of the spacecraft (MT + CMG)
- **earth pointing** of the S/C's antenna (CMG only)

2 ADCS Architecture

In this section the technical specifications of the selected ADCS components will be provided.

2.1 Attitude Sensors

2.1.1 Gyroscope - STIM202 (*Sensonor, AS*)

Table 3: *Gyro datasheet*

ARW	RRW	Sampling rate	Power	Mass	Dimensions
0.2 deg/h ^{0.5}	0.3 deg/h	1000 Hz	5.5 W	55 g	(39 × 45 × 20) mm

2.1.2 Sun Sensor - SS200 (*Hyperion Technologies, B.V.*)

Table 4: *SS datasheet*

Accuracy	FoV	Sampling rate	Power (@idle)	Power (@sampling)	Mass	Dimensions
< 1°	110°	100 Hz	< 1.5 mW	2.5 ÷ 40 mW	3 g	(24.7 × 15.0 × 3.5) mm

2.1.3 Earth Horizon Sensor - MAI-SES (*Maryland Aerospace, Inc.*)

Table 5: *EH datasheet*

Configuration	Accuracy	FoV	Voltage	Current (per sensor)	Mass	Dimensions
4 thermopile detectors	< 0.25°	7°	3.3 V	40 mA	33 g	(43.3 × 31.7 × 31.7) mm

2.2 Actuators

2.2.1 Magnetorquers - NCTR-M012 (*NewSpace Systems, Ltd.*)

Table 6: *MT datasheet*

Magnetic dipole	Residual induction	Power	Mass	Dimensions
1.19 Am ²	< 0.005 Am ²	< 800 mW	50 g	(94 × 15 × 13) mm

In order to achieve three-axis control, 3 orthogonal torque rods are employed.

2.2.2 Control Moment Gyros (*Honeybee Robotics, Ltd.*)

Table 7: *CMG datasheet*

Configuration	Angular momentum	Torque	Power (overall)	Mass	Size
4 CMGs (pyramid)	0.056 N · m · s	0.112 N · m	8 ÷ 10 W	0.6 kg (per CMG) 0.7 kg (electronics)	(48 × 48 × 91) mm

3 Model Description

3.1 Spacecraft Dynamics

In the analysis of a S/C's dynamics, one would typically de-couple orbital mechanics and attitude dynamics, due to their very different time scales. As a result we may neglect the translational component between the inertial frame and the body frame. It has been chosen to represent the S/C's attitude by means of its attitude matrix $A_{B/N}$ (also known as DCM).

3.1.1 Attitude Dynamics

The attitude of the cubesat is computed by integrating Euler's Eqs.

$$J\dot{\underline{\omega}} = J\underline{\omega} \times \underline{\omega} + \underline{u} + \underline{d} \quad (1)$$

which, using principal coordinates, can be rewritten as:

$$\begin{cases} \dot{\omega}_x = \frac{J_y - J_z}{J_x} \omega_y \omega_z + \frac{u_x + d_x}{J_x} \\ \dot{\omega}_y = \frac{J_z - J_x}{J_y} \omega_x \omega_z + \frac{u_y + d_y}{J_y} \\ \dot{\omega}_z = \frac{J_x - J_y}{J_z} \omega_x \omega_y + \frac{u_z + d_z}{J_z} \end{cases}$$

3.1.2 Orbital Mechanics

The effect of perturbations upon the orbit itself is neglected. The on-board model for determining the orbital position is hence based on the integration of the true anomaly

$$\dot{\theta} = \frac{n(1 + e \cdot \cos \theta)^2}{(1 - e^2)^{1.5}} \quad (2)$$

where $n := \sqrt{\frac{\mu}{a^3}}$.

At this point we may easily retrieve both the position and velocity vectors in the perifocal reference frame and compute the corresponding ECI coordinates by means of a proper rotation matrix:

$$\begin{aligned} \underline{\mathbf{r}}_{PF} &= r \cdot \begin{Bmatrix} \cos \theta \\ \sin \theta \\ 0 \end{Bmatrix} & \underline{\mathbf{v}}_{PF} &= \sqrt{\frac{\mu}{p}} \cdot \begin{Bmatrix} -\sin \theta \\ e + \cos \theta \\ 0 \end{Bmatrix} \\ \underline{\mathbf{r}}_{ECI} &= R_{313}^T \underline{\mathbf{r}}_{PF} & \underline{\mathbf{v}}_{ECI} &= R_{313}^T \underline{\mathbf{v}}_{PF} \end{aligned}$$

where $R_{313} := R_3[\omega] \cdot R_1[i] \cdot R_3[\Omega]$.

3.2 Disturbance Torques

3.2.1 Atmospheric Drag

The underlying idea of our modeling strategy is that of decomposing the S/C's external structure into a set of flat surfaces (defined by normal unit vectors $\hat{\mathbf{n}}_i$) and then compute the overall torque caused by drag as the superposition of each individual contribution:

$$\begin{aligned} \underline{\mathbf{d}}_{drag} &= \sum_i \underline{\mathbf{r}}_i \times \underline{\mathbf{F}}_i \\ &= \sum_i \left((\underline{\mathbf{r}}_{CP_i} - \underline{\mathbf{r}}_{CG_i}) \times \underline{\mathbf{F}}_i \right) \end{aligned}$$

where

$$\underline{\mathbf{v}}_r^N = \underline{\mathbf{v}}_{ECI} + \underline{\omega}_{earth} \times \underline{\mathbf{r}}_{ECI}$$

$$\underline{\mathbf{v}}_r = A_{B/N} \underline{\mathbf{v}}_r^N$$

$$\underline{\mathbf{F}}_i = \begin{cases} -\frac{1}{2} C_D \rho v_r^2 (\hat{\mathbf{n}}_i \cdot \hat{\mathbf{v}}_r) A_i \hat{\mathbf{v}}_r & \text{if } \hat{\mathbf{n}}_i \cdot \hat{\mathbf{v}}_r > 0 \\ \mathbf{0} & \text{if } \hat{\mathbf{n}}_i \cdot \hat{\mathbf{v}}_r \leq 0 \end{cases} \quad (3)$$

A constant value of $\rho = 1.454 \cdot 10^{-13} \frac{\text{kg}}{\text{m}^3}$ was assumed for the density, according to the model provided in [Val01]. For the drag coefficient a worst-case scenario approach was instead adopted, setting it to $C_D = 2.2$.⁽¹⁾

3.2.2 Solar Radiation Pressure

The electromagnetic radiation level is basically given by three main contributions:

- direct solar radiation ($\sim 1358 \frac{\text{W}}{\text{m}^2}$, practically constant at all altitudes)
- solar radiation reflected by Earth
- earth's own radiation

The last two contributions are instead strongly dependent on the altitude. In correspondence of our 600 km orbit we may consider $F_e = 1358 + 580 + 143.4 = 2081.4 \frac{\text{W}}{\text{m}^2} \rightarrow P = \frac{F_e}{c} = 6.938 \mu\text{Pa}$. Similar to the modeling strategy presented in 3.2.1, the cubesat is discretized using flat surfaces, each of which is associated with given specular and diffuse reflection coefficients (ρ_s and ρ_d). Then, from the knowledge of the relative Sun direction in the body frame $\hat{\mathbf{s}} = A_{B/N} \hat{\mathbf{s}}^N$, one may compute:

$$\underline{\mathbf{d}}_{SRP} = \sum_i \left((\mathbf{r}_{CP_i} - \mathbf{r}_{CG_i}) \times \underline{\mathbf{F}}_i \right)$$

where

$$\underline{\mathbf{F}}_i = \begin{cases} -PA_i(\hat{\mathbf{n}}_i \cdot \hat{\mathbf{s}}) \left[(1 - \rho_s)\hat{\mathbf{s}} + \left(2\rho_s(\hat{\mathbf{n}}_i \cdot \hat{\mathbf{s}}) + \frac{2}{3}\rho_d \right) \hat{\mathbf{n}}_i \right] & \text{if } \hat{\mathbf{n}}_i \cdot \hat{\mathbf{s}} > 0 \\ \mathbf{0} & \text{if } \hat{\mathbf{n}}_i \cdot \hat{\mathbf{s}} \leq 0 \end{cases} \quad (4)$$

3.2.3 Earth's Magnetic Field

For a precise modeling of the Earth's magnetic field, the latter might be expressed in an Earth-rotating frame as the gradient of a complicated potential function given by a series expansion of spherical harmonics. For our purposes (i.e. determining whether the chosen control strategy is robust to disturbances), a simplified modeling is actually sufficient:

$$\underline{\mathbf{b}}_N = \frac{R_{\text{earth}}^3 H_0}{r^3} [3(\hat{\mathbf{m}} \cdot \hat{\mathbf{r}}) \hat{\mathbf{r}} - \hat{\mathbf{m}}] \quad \longrightarrow \quad \underline{\mathbf{b}}_B = A_{B/N} \underline{\mathbf{b}}_N$$

where $H_0 := \sqrt{(g_1^0)^2 + (g_1^1)^2 + (h_1^1)^2}$

The Gaussian coefficients g_n^m, h_n^m are subject to time variation over the years and their experimental value is known up to 13th order.⁽²⁾

The magnetic disturbance torque is caused by the interaction between Earth's magnetic field, as given by Eq. 5, and the residual magnetic induction due to on-board currents through wirings/electronics. Such parasitic induction is difficult to model, which makes it typical to consider a worst-case scenario in which we assume $\underline{\mathbf{m}} = [0.1 \ 0.1 \ 0.1]^T \text{ Am}^2$.

The corresponding disturbance torque is hence computed as:

$$\underline{\mathbf{d}}_{\text{magn}} = \underline{\mathbf{m}} \times \underline{\mathbf{b}}_B$$

3.2.4 Gravity Gradient

As a result of the non-uniformity of the gravity field over the S/C's body, a non-negligible torque will arise. Integrating the gravitational force over the the body of the satellite will eventually yield:

⁽¹⁾ C_D values of a satellite typically ranging between 1.6 and 2.2

⁽²⁾we will consider the IGRF standard values

$$\underline{\mathbf{d}}_{\text{GG}} = \frac{3Gm_{\text{earth}}}{r^3} \cdot \begin{Bmatrix} \frac{J_z - J_y}{J_x} c_3 c_2 \\ \frac{J_x - J_z}{J_y} c_1 c_3 \\ \frac{J_y - J_x}{J_z} c_2 c_1 \end{Bmatrix} \quad (6)$$

where $\begin{Bmatrix} c_1 \\ c_2 \\ c_3 \end{Bmatrix} := A_{\text{B/L}}(:, 1)$

3.3 Attitude Sensors

3.3.1 Gyroscope

The raw measurement coming from the gyroscope will be inevitably affected by the presence of noise, which results in the presence of both a noise term and a bias term in the angular velocity output:

$$\underline{\boldsymbol{\omega}}_{\text{meas}} = \underline{\boldsymbol{\omega}} + \underline{\mathbf{n}} + \underline{\mathbf{b}} \quad (7)$$

- ARW: $\underline{\mathbf{n}} = \sigma_n \underline{\boldsymbol{\xi}}_n$ ← due to thermo-mechanical noise
- RRW: $\dot{\underline{\mathbf{b}}} = \sigma_b \underline{\boldsymbol{\xi}}_b$ ← due to electronic noise (*flicker*)

Both ARW and RRW have been modeled as a Gaussian noise,⁽³⁾ according to the specifications provided in Tab. 3.

3.3.2 Sun Sensor & Earth-Horizon Sensor

Given their more complex working principles, both SS and EH have not been simulated, unlike it was done instead for the gyro's internal dynamics. The reading of such sensors is thus simply modeled as the “true” values,⁽⁴⁾ superimposed with a random noise whose amplitude is determined by the sensor accuracy reported in Tabs. 4, 5.

3.4 Actuators

3.4.1 CMGs

CMGs generate a torque via gyroscopic effect: the rotor is tilted about an axis orthogonal to the spin axis, which results in a torque around the corresponding third orthogonal axis. Let us consider a pyramid configuration that makes use of 4 gyroscopes, in which the gimbal motor is inclined by a constant angle $\beta = 50^\circ$.

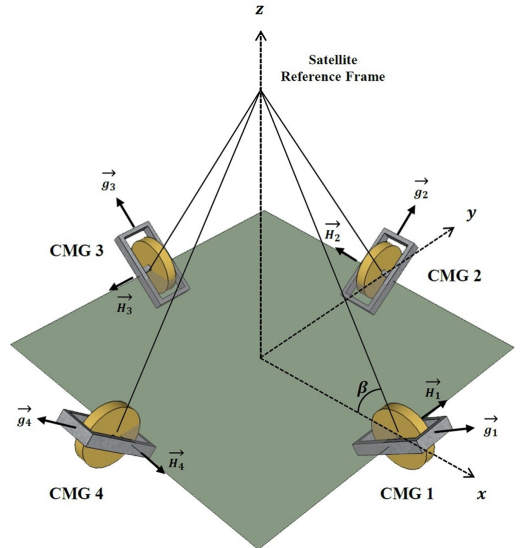


Figure 2: CMG's pyramid configuration

The angular momentum of each individual CMG may be expressed as a function of the respective tilt angle δ_i , which we may eventually rewrite in matrix form:

⁽³⁾i.e. having zero mean and $\text{std}() = \sigma_0$

⁽⁴⁾i.e. determined by the propagation of the orbit and the cubesat's attitude

$$\underline{\mathbf{h}}_{\text{CMG}} = h_R \underbrace{\begin{bmatrix} \sin \beta \cos \delta_1 & \sin \beta \cos \delta_2 & \sin \beta \cos \delta_3 & \sin \beta \cos \delta_4 \\ \sin \delta_1 & \cos \beta \cos \delta_2 & -\sin \delta_3 & -\cos \beta \cos \delta_4 \\ -\cos \beta \cos \delta_1 & \sin \delta_2 & \cos \beta \cos \delta_3 & -\sin \delta_4 \end{bmatrix}}_{:=B}$$

The dynamic equations of the system here considered (S/C + CMGs) are given by:
 $\dot{\underline{\omega}} = J\underline{\omega} \times \underline{\omega} + \underbrace{\dot{A}_R \underline{\mathbf{h}}_R + \underline{\omega} \times A_R \underline{\mathbf{h}}_R}_{\equiv \text{control torque}}$, which may be eventually solved for the tilt rates as:

$$\dot{\underline{\delta}} = -B^+ (\underline{\mathbf{u}}_{\text{id}} + \underline{\omega} \times A_R \underline{\mathbf{h}}_R) \quad (8)$$

The actual delivered torque will then correspond to

$$\underline{\mathbf{u}}_{\text{CMG}} = -B \dot{\underline{\delta}} - \omega \times A_R \underline{\mathbf{h}}_R \quad (9)$$

3.4.2 Magnetorquers

The generated magnetic dipole will be proportional to current intensity according to:

$$\underline{\mathbf{m}} = \mu N S \cdot \underline{\mathbf{I}}$$

In some cases it is possible to modulate $\underline{\mathbf{m}}$, however the small actuator here selected can only be switched on/off and change direction of the dipole, i.e. either $m = -1.19, 0, +1.19 \text{ Am}^2$.

The resulting output torque is given by:

$$\underline{\mathbf{u}}_{\text{MT}} = \underline{\mathbf{m}} \times \underline{\mathbf{b}} \quad (10)$$

4 Control & Determination Algorithms

4.1 Control Laws

4.1.1 De-Tumbling

The de-tumbling of the S/C is split in two phases.

- ~ 500 s using MTs, during which the torque rods are switched on/off according to $\underline{\mathbf{m}} = -m_{\max} \cdot \text{sgn}(\dot{\underline{\mathbf{b}}})$. However, due to the noisy nature of the magnetometer reading, the approximation $\dot{\underline{\mathbf{b}}} \approx \underline{\mathbf{b}} \times \underline{\boldsymbol{\omega}}$ is introduced. Thus $\underline{\mathbf{u}}_{\text{MT}} = -m_{\max} \cdot \text{sgn}(\underline{\mathbf{b}} \times \underline{\boldsymbol{\omega}}) \times \underline{\mathbf{b}}$.
- a few seconds using CMGs, to de-tumble completely the cubesat, according to the simple ideal law: $\underline{\mathbf{u}}_{\text{id}}^{\text{CMG}} = -k\underline{\boldsymbol{\omega}}$.

4.1.2 Tracking: Earth Pointing

Let us consider the problem of tracking a generic time-varying desired attitude A_d as well as maintaining a desired angular velocity $\underline{\boldsymbol{\omega}}_d$. If we define the corresponding attitude and angular velocity errors $A_e = AA_d^\top$, $\underline{\boldsymbol{\omega}}_e = \underline{\boldsymbol{\omega}} - A_e \underline{\boldsymbol{\omega}}_d$ then a suitable DCM-based control law would be:⁽⁵⁾

$$\underline{\mathbf{u}}_{\text{id}} = -k_1 \underline{\boldsymbol{\omega}}_e - k_2 [A_e^\top - A_e]^\vee + \underline{\boldsymbol{\omega}} \times J \underline{\boldsymbol{\omega}} + J(A_e \dot{\underline{\boldsymbol{\omega}}}_d - \underline{\boldsymbol{\omega}}_e \times A_e \underline{\boldsymbol{\omega}}_d) \quad (11)$$

In our specific case, the desired attitude at a given instant will be simply given by the inertial-to-LVLH rotation matrix, namely:

$$A_d \equiv A_{\text{L/N}} = \begin{bmatrix} \cos(\theta(t)) & \sin(\theta(t)) & 0 \\ -\sin(\theta(t)) & \cos(\theta(t)) & 0 \\ 0 & 0 & 1 \end{bmatrix} \begin{bmatrix} 1 & 0 & 0 \\ 0 & \cos(i(t)) & \sin(i(t)) \\ 0 & -\sin(i(t)) & \cos(i(t)) \end{bmatrix}$$

For Earth pointing the set of CMGs alone will be employed.

4.2 Attitude Determination Algorithm

We will make use of the **SVD** method, which has been developed within the framework of Wabha's problem. The latter consists in minimizing the weighted cost function

$$\mathcal{J} = \frac{1}{2} \sum_{i=1}^N \alpha_i \|\hat{\underline{\mathbf{v}}}_{B_i} - A_{\text{B/N}} \hat{\underline{\mathbf{v}}}_{N_i}\|$$

in which N sensor measurements $\hat{\underline{\mathbf{v}}}_{B_i}$ are available,⁽⁶⁾ along with the corresponding estimations $A_{\text{B/N}} \hat{\underline{\mathbf{v}}}_{N_i}$ computed using on-board models; in addition the weighting coefficients α_i are chosen based on the accuracy of each sensor. The algorithm makes use of the following procedure:

$$\begin{aligned} B &:= \sum_{i=1}^N \alpha_i \hat{\underline{\mathbf{v}}}_{B_i} \hat{\underline{\mathbf{v}}}_{N_i}^\top \\ B &\stackrel{\text{SVD}}{=} U S V^\top \\ M &= \begin{bmatrix} 1 & 0 & 0 \\ 0 & 1 & 0 \\ 0 & 0 & \det U \cdot \det V \end{bmatrix} \\ A_{\text{B/N}} &= U M V^\top \end{aligned} \quad (12)$$

⁽⁵⁾ $[\cdot]^\vee$ denotes the inverse-hat operator, i.e. it maps a skew-symmetric matrix back to its generating vector

⁽⁶⁾ $\hat{\underline{\mathbf{v}}}$ denotes the direction of an inertial reference, e.g. the Sun, Earth's center, a star, etc.

4.3 Noise Filtering

Both the gyro output and the raw estimated attitude will be inevitably affected by the presence of noise. Making use of a frequency-based LPF would be unsuitable for real time processing. Indeed, filtering the original signal would result in an excessive phase delay, which in turn translates into a delayed control law. Thus, it has been chosen to employ a **state observer**, that basically acts as a filter but with no delay. For instance, in the event of gyro-noise filtering:

$$J\dot{\hat{\omega}} = J\hat{\omega} \times \hat{\omega} + \underline{u} + \underline{d} + \alpha_1(\hat{\omega} - \underline{\omega}_{\text{raw}}) \quad (13)$$

where $\alpha_1 < 0$ is a tuning parameter.

An analogous procedure is carried out for filtering the raw attitude estimation.

5 Results

5.1 Disturbance Torques

We will now provide the trend of the various disturbance torques over two complete **control-free** orbits,⁽⁷⁾ with the following initial conditions:

$$\underline{\omega}(0) = \begin{Bmatrix} 5 \\ 10 \\ -7 \end{Bmatrix} \frac{\text{deg}}{\text{s}} \quad A_{\text{B/N}}(0) = \mathbb{I}$$

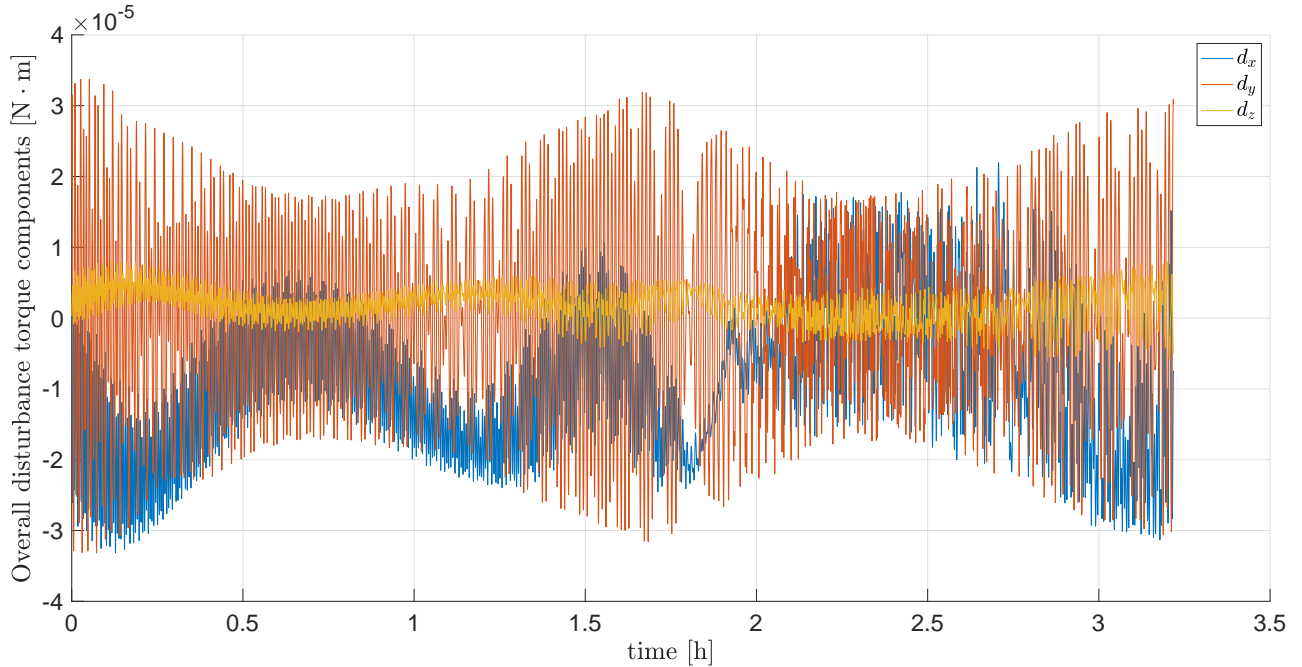


Figure 3: Components of the overall disturbance torque

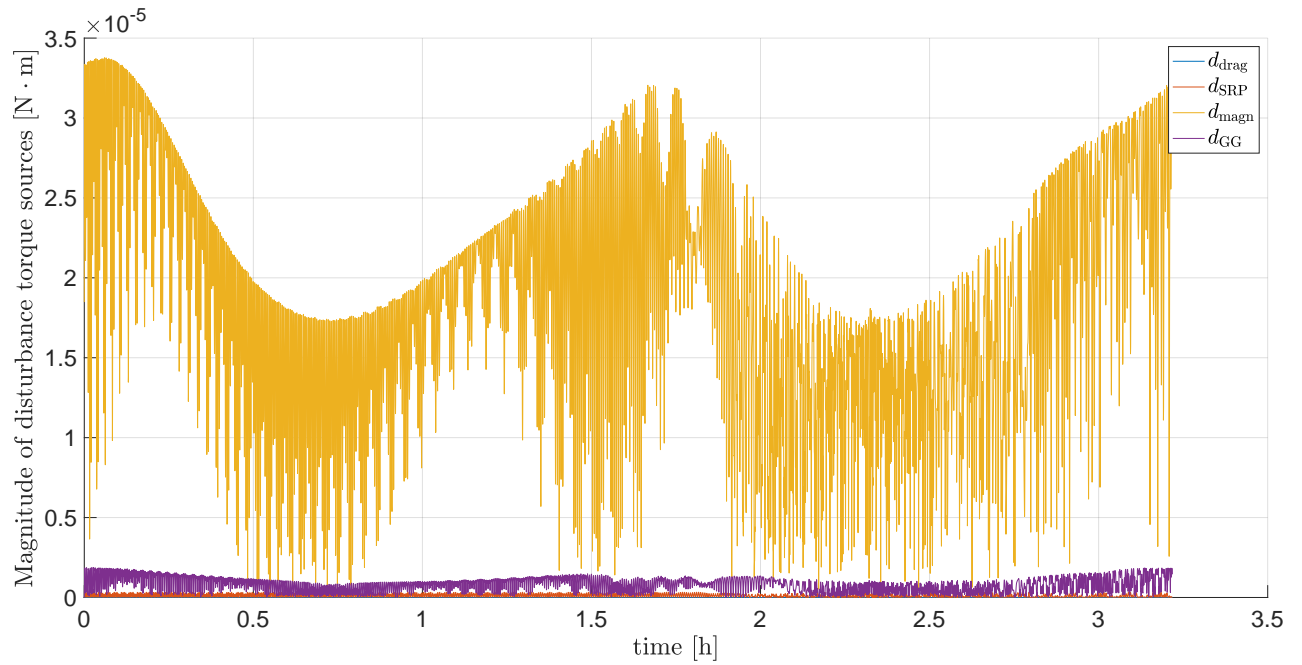


Figure 4: Disturbance torque sources

⁽⁷⁾recall that the orbital period is given by $T = 2\pi\sqrt{\frac{a^3}{\mu}} = 5792 \text{ s} = 1 \text{ h } 37 \text{ min}$

Figs. 4 and 5 highlight that magnetic torque will be largely dominant, while the contribution due to drag is actually negligible compared to other environmental disturbances.

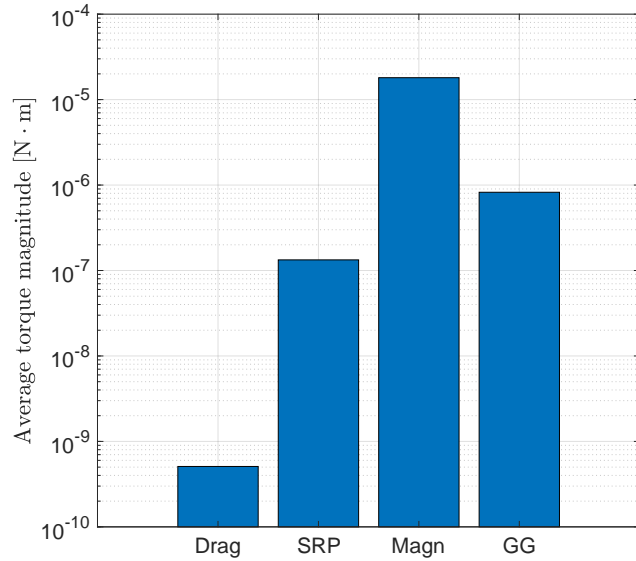


Figure 5: Order of magnitude of disturbance torques

5.2 De-Tumbling

Let us assume the same reference initial conditions provided in 5.1. As already stated in 4.1.1, the de-tumbling maneuver will consist in a long phase during which magnetorquers are employed, followed by a short CMG phase once the tumbling rate becomes low enough to guarantee a reliable operation of SS and EH. The maneuver will actually start 10 s after the initial time, in order to wait for a stable gyro reading.

5.2.1 Dynamics

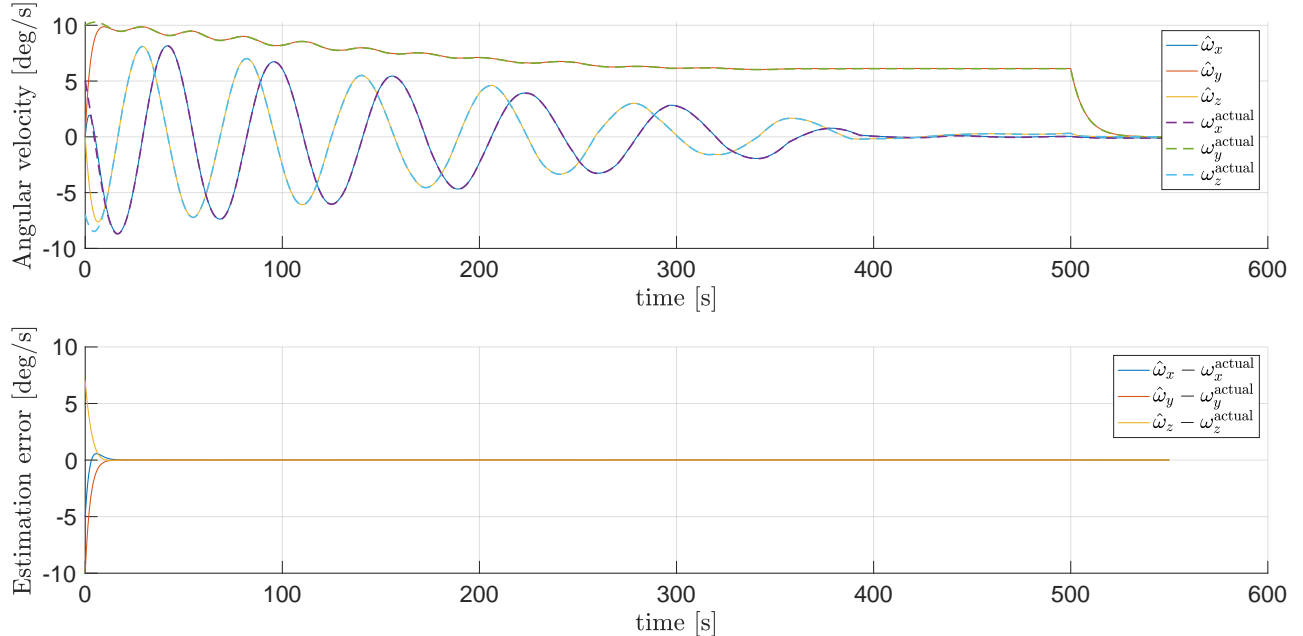


Figure 6: Angular velocity and related estimation error

From Fig. 6 it can be seen that the MTs alone do not allow a complete de-tumbling of the S/C; in particular they have poor effectiveness for de-tumbling the y-component. After 490 s of operation (i.e. at $t = 500$ s), the MTs are switched off, while CMGs are activated and all the tumbling-rate

components are brought to practically zero.

The related estimation error will soon converge to zero, after about 10 s.

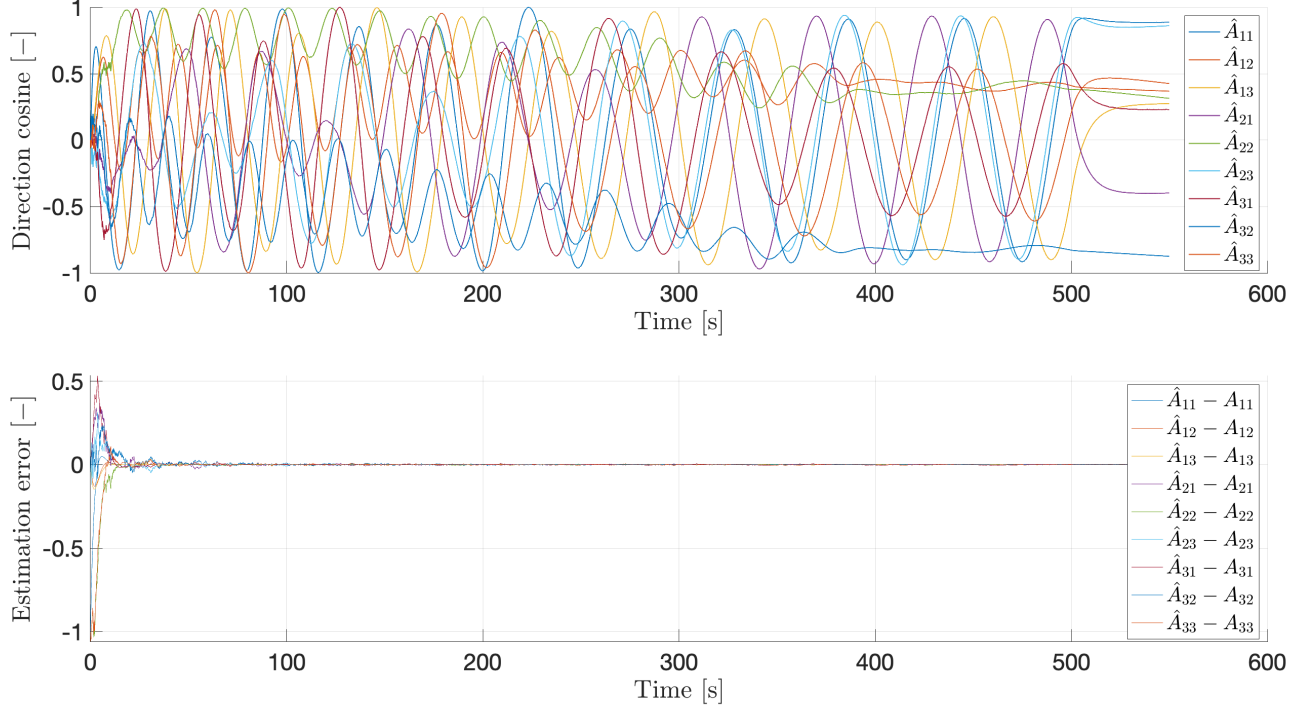


Figure 7: Attitude matrix and related estimation error

Fig. 7 shows how the direction cosines of the attitude matrix will progressively damp their oscillation as the cubesat undergoes de-tumbling. Once complete de-tumbling is achieved, the components of $A_{B/N}$ become almost constant: at this point the only source of variation of the relative attitude w.r.t. an inertial frame is the orbital motion.

5.2.2 Control

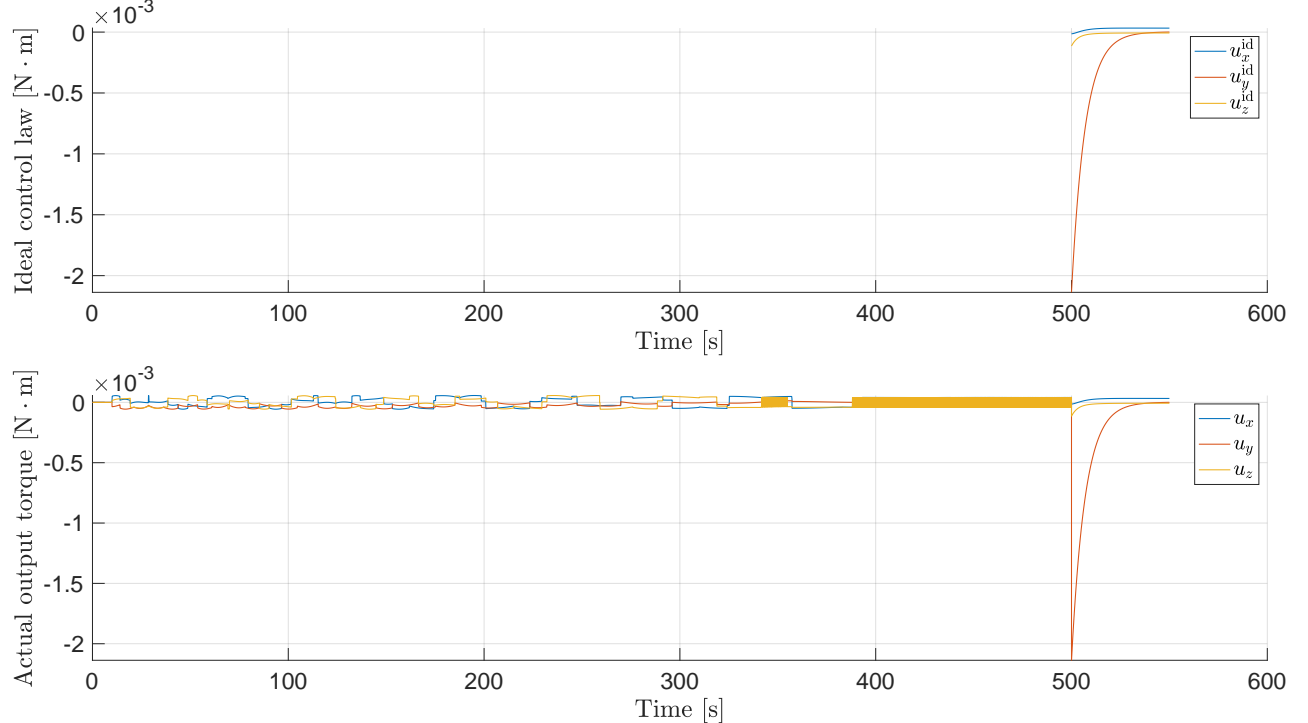


Figure 8: Ideal control law and actual output torque

Fig. 8 highlights the pulsed operation of our small magnetorquers, whose magnetic dipole cannot be modulated in amplitude. The effective output torque will clearly be subject to slight variations, depending on the S/C's attitude w.r.t. Earth's magnetic field. Note that the ideal control law has only been plotted for the operation of CMGs, because as long as the MTs alone are used, the ideal and actual torques will basically coincide according to our simplified model.

5.3 Earth Pointing

We will assume to start the pointing maneuver with the S/C in a de-tumbled state, i.e. zero angular velocity. The initial attitude matrix is instead the same as the one obtained at the end of the simulation in 5.2.

Also in this case, we will have to wait 10 s before initiating the maneuver, in order to achieve a stable reading of all our sensors (gyro, SS, EH).

5.3.1 Dynamics

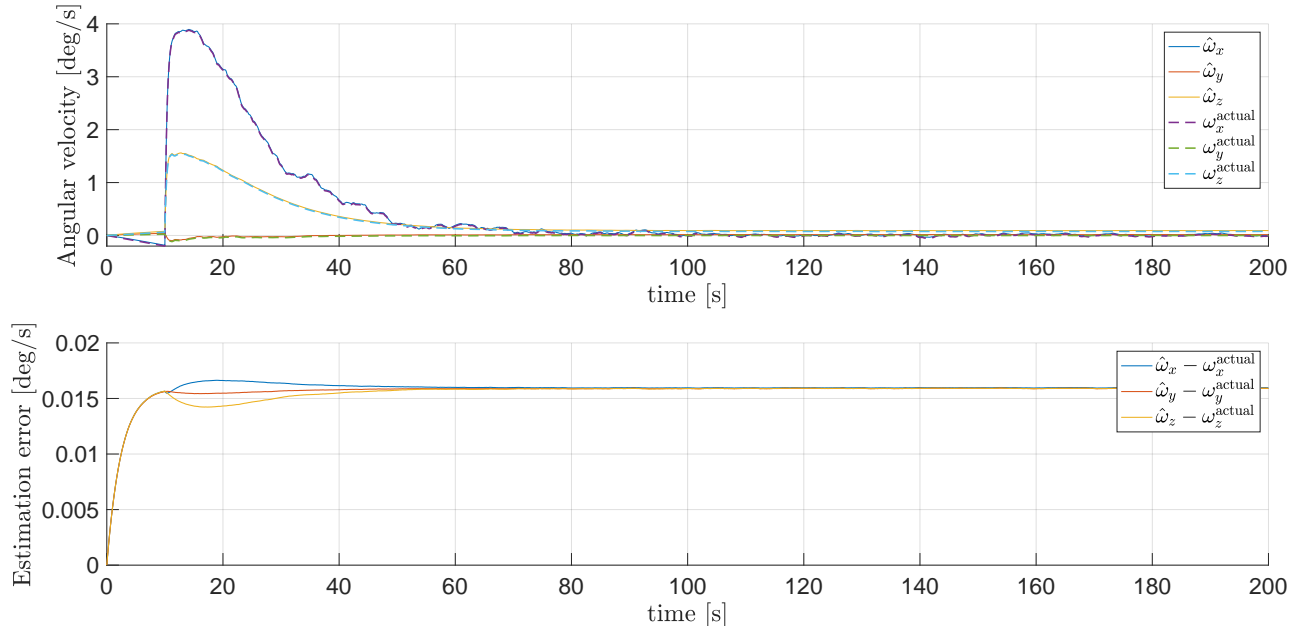


Figure 9: Angular velocity and related estimation error

In Fig. 9 it can be observed that an initial angular velocity increase is needed in order to align the S/C with the desired attitude. The angular velocity is then progressively damped as the attitude approaches the desired one.

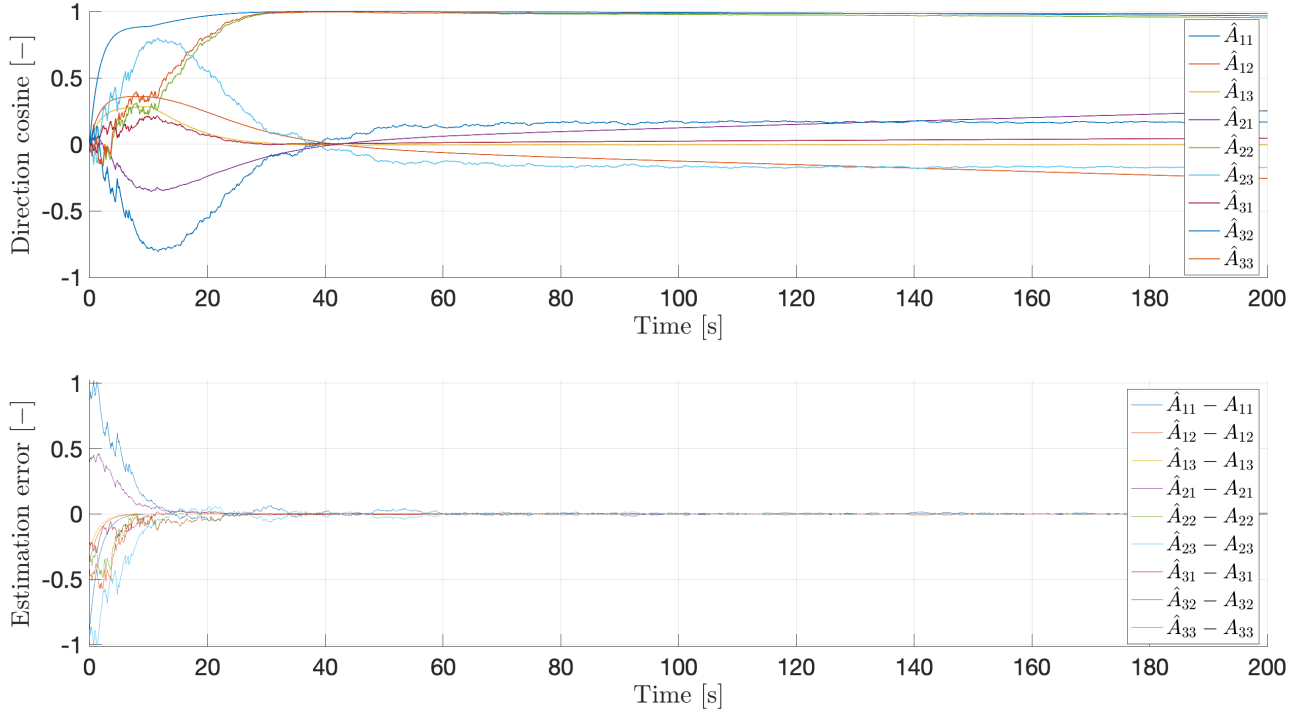


Figure 10: Attitude matrix and related estimation error

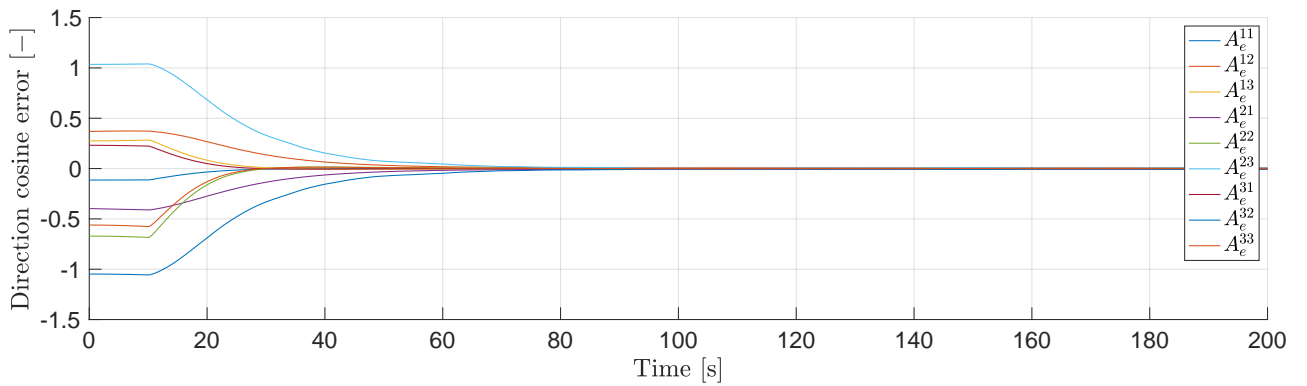


Figure 11: Attitude error w.r.t. the desired attitude

By inspecting Fig. 11 we may conclude that a close to perfect alignment is achieved after ~ 80 s (only 70 s after CMGs are turned on).

5.3.2 Control

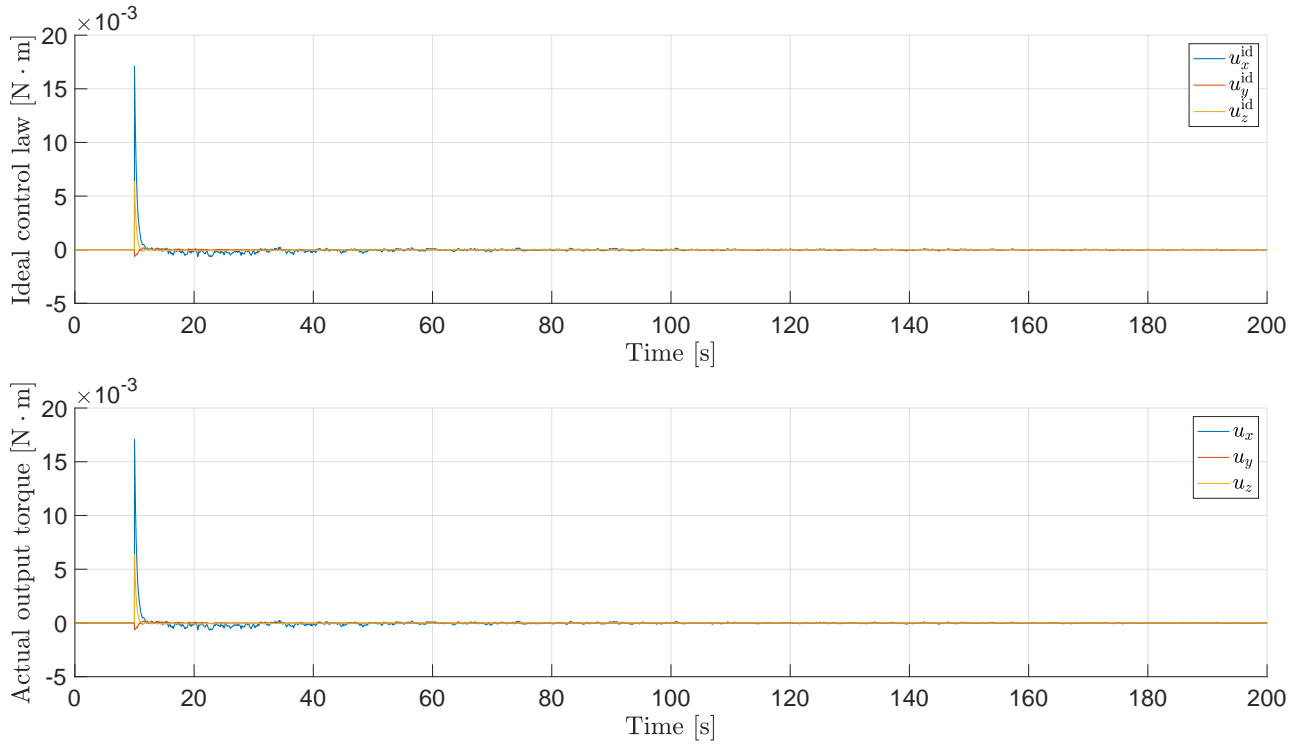


Figure 12: Ideal control law and actual output torque

It turns out that the effective output torque is very close to the ideal control we designed, which is achieved thanks to the practically continuous operation of CMGs.

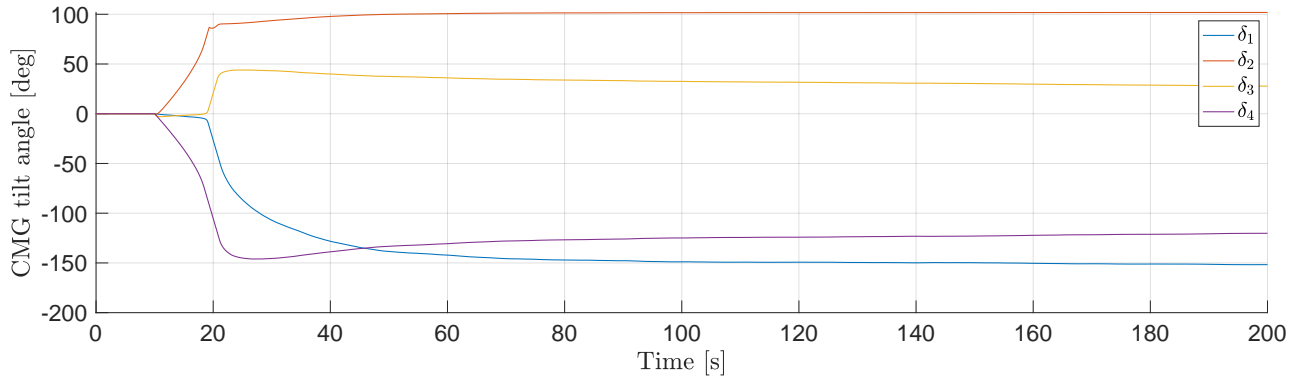


Figure 13: CMG tilt angles

The tilt angles reported in Fig. 13 become basically constant past $t = 80$ s, which is indeed consistent with the trend of the attitude error.

6 Conclusions

We may eventually conclude that both the de-tumbling and Earth-pointing tasks are successfully completed. The designed control laws are stable and robust to disturbances, even in the presence of noisy raw sensor readings.

The magnetic torque rods have poor effectiveness for the purpose of de-tumbling the y-component of angular velocity, which makes it necessary to employ a different class of actuators as well.

The chosen model of CMG appears to largely overcome the performance requirements for controlling the small 6U cubesat.⁽⁸⁾ It nevertheless turns out to be the smallest device currently available on the market.

⁽⁸⁾max torque of Honeybee Robotics' CMG: 0.112 N · m, compared to a peak required torque of only 0.020 N · m achieved during our simulation

References

- [Mar14] F Landis Markley and John L Crassidis. *Fundamentals of spacecraft attitude determination and control*. Vol. 33. Springer, 2014.
- [Val01] David A Vallado. *Fundamentals of astrodynamics and applications*. Vol. 12. Springer Science & Business Media, 2001.
- [Wer12] James R Wertz. *Spacecraft attitude determination and control*. Vol. 73. Springer Science & Business Media, 2012.
- [Wie08] Bong Wie. *Space vehicle dynamics and control*. American Institute of Aeronautics and Astronautics, 2008.